Int J Adv Manuf Technol (2017) 91:389–397
DOI 10.1007/s00170-016-9752-4

ORIGINAL ARTICLE

Effects of rotation rate on microstructure and mechanical properties of friction stir-welded Mg-5Al-1Sn magnesium alloy

Fusheng Pan [1,2] · Anlian Xu [1] · Junhua Ye [1] · Aitao Tang [1] · Xianquan Jiang [2] · Yang Ran [3] · Weiwei Du [2]

Received: 1 September 2016 / Accepted: 7 November 2016 / Published online: 21 November 2016

Abstract Mg-Al-Sn magnesium alloys have bright future in application because of good properties without rare earth elements. To study the effects of rotation rate on microstructures and mechanical properties of Mg-5Al-1Sn alloy after friction stir welding (FSW), extruded plates were butt welded by FSW with various rotation rates at constant other parameters. The results showed that after FSW, $Mg_{17}Al_{12}$ phase with poor thermal stability was dissolved, while Mg_2Sn phase remained due to high dissolution point and good thermal stability. The hole-type defects were observed at 600 rpm, and the weld joint was with no defects at 800~1100 rpm. The weld joint at 800 rpm gave a maximum ultimate tensile strength (UTS), which was 91% of the base material (BM). After FSW, both UTS and elongation of weld joints decreased compared with the BM, caused by the soften region between nugget zone (NZ) and thermo-mechanically affected zone (TMAZ), the dissolution of $Mg_{17}Al_{12}$ phases, the residual stress and dislocation content in the TMAZ, and the textural variation. With increasing rotation rate from 600 to 1100 rpm, the UTS of weld joints first increased and then decreased, while the elongation kept mostly unchangeable due to the common action of multifactors.

✉ Fusheng Pan
fspan@cqu.edu.cn

✉ Anlian Xu
xuanlian05@163.com

[1] College of Materials Science and Engineering, Chongqing University, Chongqing, China

[2] Chongqing Academy of Science and Technology, Chongqing, China

[3] Chongqing Institute of Optics Mechanics, Chongqing, China

Keywords Friction stir welding · Mg-5Al-1Sn magnesium alloy · Mechanical properties · Rotation rate · Microstructure characteristics

1 Introduction

For magnesium alloys, large-scale commercial application has been driven by a reliable welding process. However, conventional fusion welding has some problems such as porosity, hot cracking, oxidation, and high residual stress, which obstruct the application of magnesium alloys [1]. Friction stir welding (FSW) is a green solid-state welding technology, and it is considered a promising joining method for aluminum alloys [2, 3], magnesium alloys [4–6], and others [7]. Nowadays, FSW of various magnesium alloys was investigated such as AZ31 [8, 9], AZ91 [4], and AM20 [6]. Effects of welding speed, rotational speed, and probe length on the quality of friction stir-welded joints of AZ31 magnesium alloy were reported by Cao and Jahazi [10, 11]. However, mechanical properties of conventional Mg-Al-Zn series alloys are not ideal, which limits their application. Magnesium alloys containing rare earth element (REE) such as AE42 [12], ZEK100 [13], and ZE41A [14] were proven to have better performances compared with the alloy without REE, and the weld joints by FSW were with no defects and good properties. Although the addiction of REE is an effective method in improving properties of magnesium alloys, the REE is expensive.

In recent years, Mg-Al-Sn series alloys have come to the foreground because of high mechanical properties without any rare earth components [15, 16]. The researches have been concentrated on the solidification microstructure and mechanical properties [17], compositional optimization [18], and the effect of strain-induced precipitation on dynamic

recrystallization [19] for Mg-Al-Sn alloys. However, there are limited reports on the welding of Mg-Al-Sn alloys. In the previous studies [16, 20], we reported that Mg-Al-Sn alloys were successfully welded by FSW, and the influence of FSW on microstructure and mechanical properties of magnesium alloy Mg-5Al-3Sn was also studied. While the effect of rotation rate on microstructure and mechanical properties of friction stir-welded Mg-Al-Sn alloys was seldom reported. We all know that a reliable welding process is vitally important to the commercial application of Mg-Al-Sn alloys. So, the hot-extruded Mg-5Al-1Sn alloy plates were welded by FSW with various rotation rates in this study, and the objective of the study was to clarify the influence of rotation rate on microstructure and mechanical properties of Mg-5Al-1Sn alloy joints after FSW.

1.1 Experimental details

The hot-extruded plates of Mg-5Al-1Sn magnesium alloy, with dimensions of 150 mm (length) × 50 mm (width) × 3 mm (thickness) and chemical composition of 4.5~5.5% Al, 0.7~1.3% Sn, and 0.2~0.4% Mn and balance Mg in weight percent, were butt welded by FSW in the direction parallel to the extruding direction. Before friction stir butt welding, surface oxides were removed by manual power brush followed by surface cleaning with ethanol. A simple FSW tool made from H13 steel with a concave shoulder 10 mm in diameter, a cylindrical threaded pin 4 mm in diameter and 2.8 mm in length, and a tool tilt angle of 2.5° was used in the study. In the previous experiments, a large number of tests showed that the welding speed was optimized by 150 mm min^{-1} with various rotation rates for friction stir-welded Mg-5Al-xSn ($x = 1.3$) alloy to achieve better mechanical properties, and it has been verified in the previous study [16]. So in the present research, the constant welding speed was 150 mm min^{-1}. Rotation rates were varied from 600 to 1100 rpm, i.e., 600, 800, 1000, and 1100 rpm. And, the weld joints of Mg-5Al-1Sn alloy after FSW were, respectively, denoted as the 600-, 800-, 1000-, and 1100-rpm welds in this study.

The weld joints were nondestructive evaluation tested by CDZ-320ZD-A X-ray radiography. Samples for microstructural characterization were cut perpendicular to the welding direction (i.e., perpendicular to the extruding direction). The samples were then ground without polishing and etched for 15 s in the reagent made of 5 g picric acid, 5 ml acetic acid, 100 ml ethanol, and 10 ml distilled water to reveal the microstructure of the joints. The microstructures were observed by a LEICA DMI 5000-M optical microscope and a JEOL 7800F scanning electron microscope (SEM) at 20 kV equipped with an INCA Energy 350 energy-dispersive X-ray spectroscopy (EDS) analysis system. After been grounded by SiC papers, XRD analysis of the samples was tested by Rigaku D/max 2500 PC X-ray diffractometer at 60 kV and 30 mA with a sample tilt angle ranging from 10 to 90°. Thermal properties of the samples were examined by differential scanning calorimetry (DSC) at a heating rate of 10 °C/min and an argon flow rate of 50 ml/min. Hardness at transverse direction was measured with a 100 g load for a 10 s. Transverse tensile test samples were cut perpendicularly to the welding direction from the joints. The configuration and size of the transverse tensile specimens were prepared according to ASTM standard E8M-15a, with the 50-mm gauge length. Tensile tests were carried out on a Sansi CMT-5105 mechanical tester using a crosshead speed of 0.5 mm min^{-1} at room temperature. To ensure high accuracy and reliability, all the weld joints were tested and recorded three times and were taken average. The fracture surface of transverse tensile specimens was observed by a VEGA3 SEM. Figure 1 shows the schematic illustration of the FSW process. In Fig. 1, NZ, TMAZ, HAZ, and BM in the weld cross section represent the nugget zone, thermo-mechanically affected zone, heat-affected zone, and base material, respectively. And, the advancing side is marked as AS and the retreating side as RS.

2 Results

2.1 Weld appearance

Figure 2 shows the surface appearance of Mg-5Al-1Sn weld joints after FSW at various rotation rates under a constant welding speed of 150 mm min^{-1}. It is seen that the welds are without macrodefects such as excessive flash, galling, void, and lack of fill on the surface of welds. X-ray radiography images of the weld joints after FSW were also shown in Fig. 2. There is no evidence defect in the welds and on the surface of welds. It is observed that the extruded Mg-5Al-1Sn alloy has good formability and weldability by FSW.

The weld joints were further evaluated by cross-section check because tiny flaws were difficult to be detected by X-ray radiography. Figure 3a–d shows the cross-sectional macrostructures of friction stir welds at various rotation rates. It is shown that all the weld joints were defect free expect at rotation rate of 600 rpm. When the rotation rate was at 600 rpm,

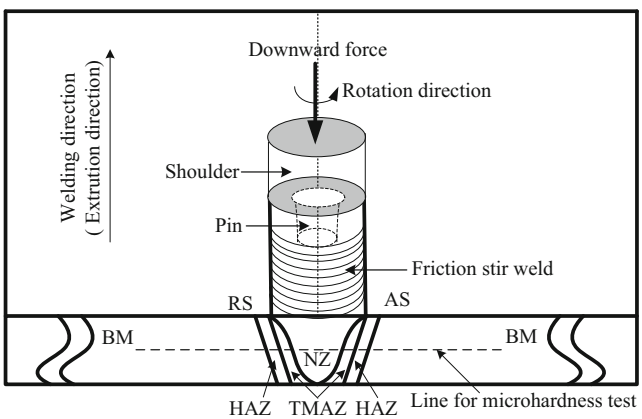

Fig. 1 Schematic illustration for the FSW process

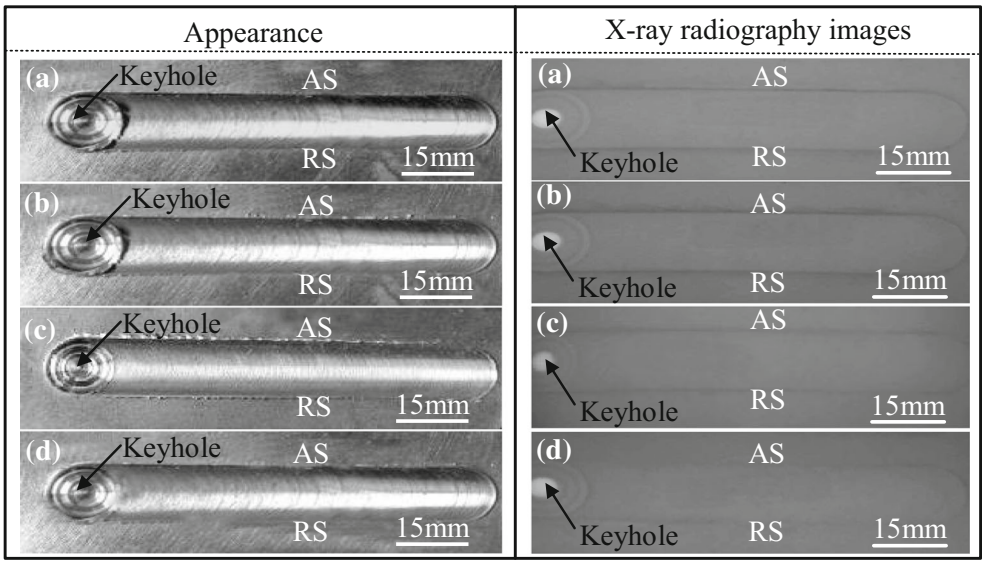

Fig. 2 Appearance and X-ray radiography images of the welds at rotation rate of **a** 600 rpm, **b** 800 rpm, **c** 1000 rpm, and **d** 1100 rpm

some hole-type defects were observed in the cross-sectional weld joints. So, there was no defect in the weld joint when the rotation rate was between 800 and 1100 rpm, while there were hole-type defects at lower rotation rate of 600 rpm.

2.2 Mechanical properties

Figure 4 shows the mechanical properties of the BM and weld joints with various rotation rates tested at room temperature. The ultimate tensile strength (UTS) and elongation of the BM were tested to be about 285 MPa and 18.7%, respectively. It is seen from Fig. 4 that both UTS and elongation of the weld joints decreased compared with that of the BM regardless of rotation rate, especially the elongation sharply decreased. The maximum value of UTS for weld joints was 258 MPa at the rotation rate of 800 rpm, which was 91% of the BM strength. While the minimum value of UTS was 223 MPa, which was just 78% of the BM strength, at the rotation rate of 600 rpm. For the rotation rate of 800~1100 rpm, the UTS of weld joints was between 87 and 91%. It is also found that the UTS of weld joints first increased and then decreased with increasing rotation rate from 600 to 1100 rpm at a constant welding speed of 150 mm min^{-1}, while the elongation had no obvious changes. Figure 5 shows the fracture morphologies of the tensile specimens for weld joints. All of the tensile specimens failed at the boundary between the NZ and TMAZ at the AS with basically 45° shear fracture. Figure 6 shows the typical SEM micrographs of tensile fracture surfaces for the BM and the 800-rpm weld after FSW. As shown in Fig. 6a, the BM displayed the fracture features of dimples together with some tear ridges. While the tensile fracture of the weld joint was mixture of cleavage-like and dimple-like, as illustrated in Fig. 6b.

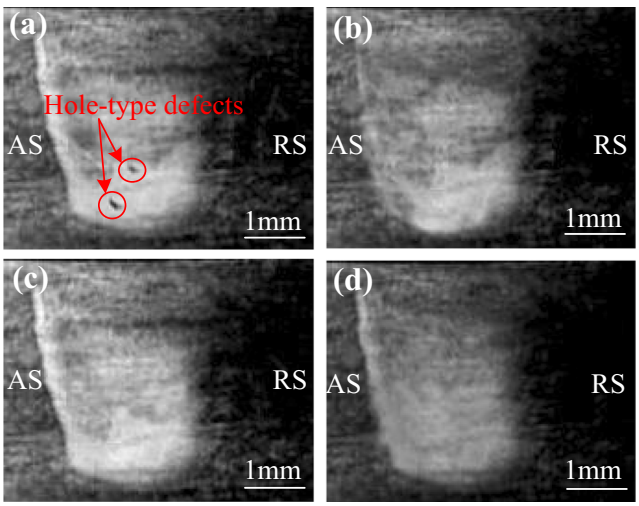

Fig. 3 Cross-sectional macrostructures of **a** the 600-rpm weld, **b** the 800-rpm weld, **c** the 1000-rpm weld, and **d** the 1100-rpm weld

Figure 7 shows the typical hardness profile across the weld center measured along the mid-thickness (indicated by dotted lines in Fig. 1). The pin and shoulder diameters were also shown in this figure. Roughly speaking, the pin diameter indicated the NZ of weld joint, whereas the shoulder diameter delineated the regions most affected by heat. From this figure, the hardness value of the BM fluctuated between 68 and 73 Hv. It is seen that the hardness value in the NZ was slightly higher than that of the BM, and the lowest hardness located in the region between NZ and TMAZ at AS but not at RS, irrespective of rotation rate. Under a constant rotation rate of 150 mm min^{-1}, with increasing rotation rate from 600 to 1100 rpm, the hardness in the NZ of weld joints had no obvious changes.

2.3 Microstructure characteristics

The microstructures in the transverse cross section of weld joints at different zones are shown in Fig. 8. According with other alloys, there were four zones in the friction stir weld

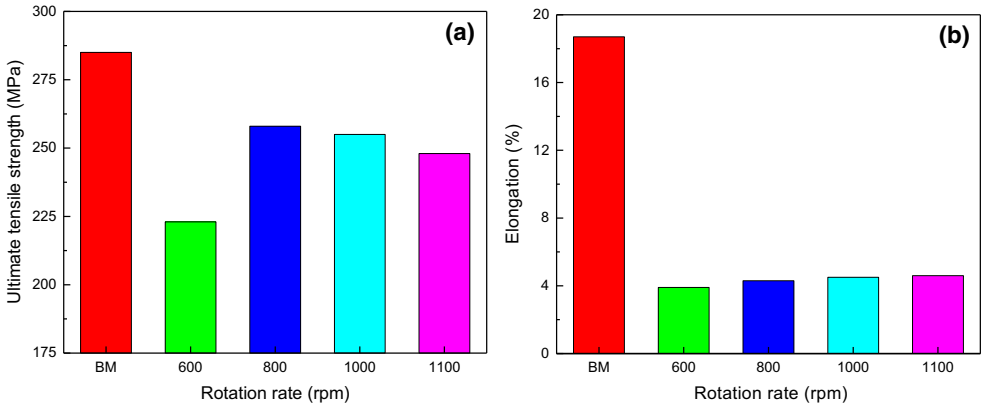

Fig. 4 Effects of rotation rates on the ultimate tensile strength (**a**) and elongation (**b**) of weld joints

joints of Mg-5Al-1Sn alloy, which were the NZ, TMAZ, HAZ, and BM. The as-received BM showed a typical deformation microstructure with equiaxed grains with α-Mg matrix and precipitated phases, which was formed in the hot extrusion process (Fig. 8a). The average grain size of the BM was about 10 μm. At the rotation rate of 800 rpm and welding speed of 150 mm min^{-1}, the average grain size of the HAZ in the weld joints was about 10.8 μm, which was slightly larger than that of the BM, as shown in Fig. 8b. Some grains were refined and others were elongated in the TMAZ of the friction stir weld (Fig. 8c), with average grain size of about 11.3 μm. The average grain size of the NZ in the weld joint was about 8.3 μm, as shown in Fig. 8e.

The microstructures in the NZ at various rotation rates are shown in Fig. 8d–g. It is clearly evident from these figures that the grains in the NZ were equiaxed microstructures, which were smaller than that of the BM, irrespective of rotation rate. When the rotation rate was at 600 rpm, there were several hole-type defects in the NZ. With increasing rotation rate from 800 to 1100 rpm, no obvious defects were observed and average grain size of the NZ increased. The average grain size of the NZ in the 800- and 1100-rpm welds were 5.6 and 8.8 μm, respectively. Figure 9 shows the SEM microstructures in the BM and NZ of friction stir welds at various rotation rates. Figure 10 shows the XRD analysis results of the BM and weld joints at various rotation rates at a constant welding speed of 150 mm min^{-1}. It can be seen that $Mg_{17}Al_{12}$ and Mg_2Sn phases were observed in the BM, while $Mg_{17}Al_{12}$ phase dissolved into α-Mg matrix and Mg_2Sn phase remained after FSW. It is also found that Mg_2Sn phase particles was refined and distributed uniformly. No obvious variation was observed for the second phase (Mg_2Sn) particles with increasing rotation rate from 800 to 1100 rpm. Figure 11 shows the thermodynamic data of the BM and NZ in the 800-rpm weld found by DSC scans. Three peaks were observed in the BM corresponding with the α-Mg matrix melting, Mg_2Sn phase, and $Mg_{17}Al_{12}$ phase transformations. While there was not a peak of $Mg_{17}Al_{12}$ phase in the NZ of weld joints after FSW. It is seen that the $Mg_{17}Al_{12}$ phase was dissolved and Mg_2Sn phase still remained, which conformed to the XRD and SEM analysis results.

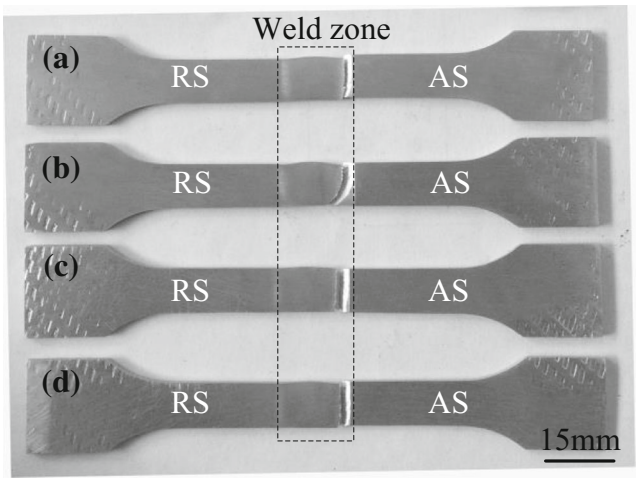

Fig. 5 Macroscopic images showing typical fracture locations of the weld joints at rotation rate of **a** 600 rpm, **b** 800 rpm, **c** 1000 rpm, and **d** 1100 rpm

3 Discussions

3.1 Microstructure evolution

The BM (Fig. 8a) is composed of equiaxed grains with α-Mg matrix and precipitated phases, which is consistent with the typical deformation microstructure formed in the hot extrusion process [21]. The $Mg_{17}Al_{12}$ phase and Mg_2Sn phase are observed in the BM (Fig. 9a), which conforms to the recent studies [21]. The microstructure of Mg-Al-Sn alloys consists of α-Mg phase, $Mg_{17}Al_{12}$ phase, and Mg_2Sn phase, and the amount of $Mg_{17}Al_{12}$ phase and Mg_2Sn phase increase with increasing the content of Al and Sn, as reported by Luo et al. [17]. After FSW, the HAZ (Fig. 8b) of weld joints is heated sufficiently without plastic deformation of grains during FSW, so the grains in the HAZ are with slightly bigger than that of the BM [22]. Microstructures of the TMAZ (Fig. 8c) are composed of fine equiaxed grains and stretched grains. The

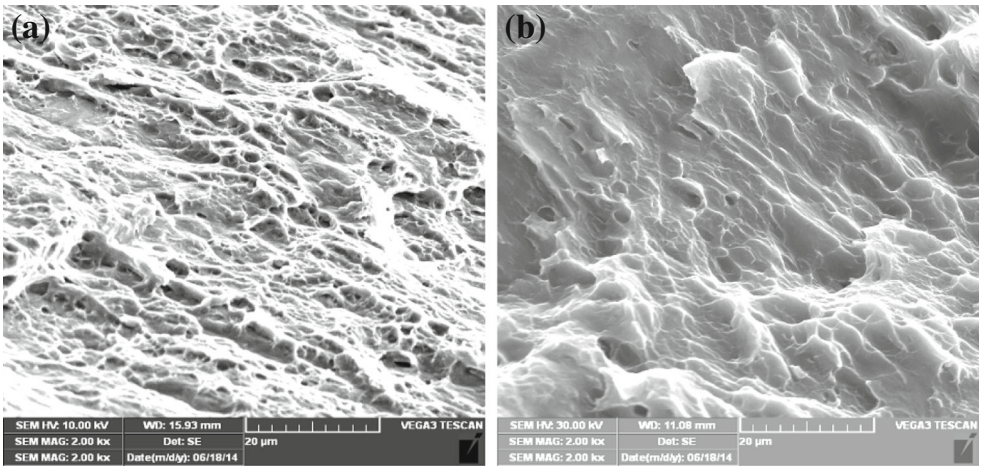

Fig. 6 Typical SEM micrographs of tensile fracture surfaces for **a** the BM and **b** the 800-rpm weld

TMAZ is under sufficient heating, softened and high process forces during FSW, so the grains in the TMAZ are with plastic deformation of the original grain structure, as it conforms to the previous study [21]. While there is lower heating temperature and weaker mechanical stirring in the TMAZ than that of the NZ. The NZ (Fig. 8d–g) of weld joints is composed of an equiaxed microstructure, and the grains in the NZ are much smaller than that of the BM because of dynamic recrystallization induced by sufficient heating and intense plastic deformation, as reported by the previous researchers [5, 23, 24]. It is widely accepted that the temperature in the NZ during FSW is lower than the melting point of the BM but higher than the recrystallization temperature [23, 25]. The temperature in the NZ of magnesium alloys during FSW can reach 400~500 °C [26–29]. Comparing with the BM, $Mg_{17}Al_{12}$ phase disappears and there are α-Mg phase and Mg_2Sn phase in the NZ of Mg-5Al-1Sn alloy weld joints (Fig. 9b–d) after FSW. Previous studies have shown that the eutectic $Mg_{17}Al_{12}$ phase with poor thermal stability can dissolve into α-Mg matrix during FSW [30]. While Mg_2Sn phase with the melting point of 772 °C has better thermal stability than $Mg_{17}Al_{12}$ phase, so Mg_2Sn phase can remain in the NZ after FSW.

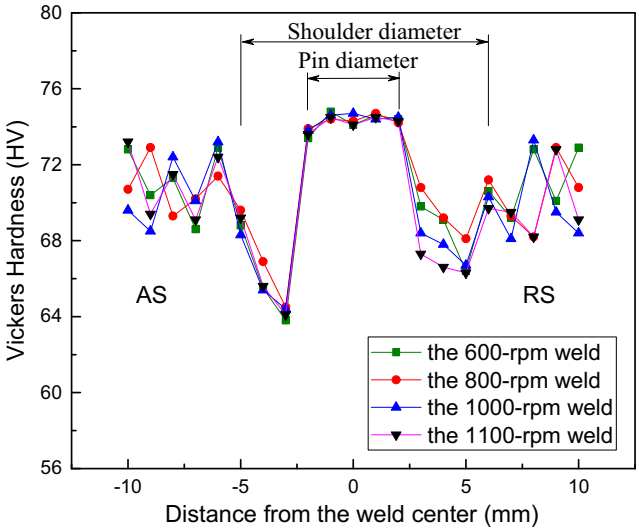

Fig. 7 Hardness profile of the friction stir weld along mid-thickness

In principle, the formation of weld joints during FSW is by means of heat produced by friction and plastic work, using a rotation tool to locally soften a workpiece [22]. The rotation rate and welding speed are two the most important process parameters. The relationship between the nugget temperature and process parameters during FSW for aluminum and magnesium alloys was deduced by Commin et al. [9]. When the rotation rate decreases at a constant welding speed, both nugget temperature and heat input decrease accordingly. If the rotation rate is too slow (such as 600 rpm for the magnesium alloy Mg-5Al-1Sn) when the welding speed is constant, it is unable to generate sufficient heat and adequate metal transportation during FSW, so that the hole-type defects appear in the weld joints (Fig. 8d). The defects can markedly influence the tensile properties of weld joints.

For the magnesium alloy Mg-5Al-1Sn, no defect is observed in the weld joints after FSW (Fig. 8e–g) because of enough heat and sufficient metal transportation. With increasing rotation rate from 800 to 1100 rpm, the grain size of the NZ in weld joints increases because of different heat input at various rotation rates during FSW. When the welding speed is constant, the nugget temperature and heat input will increase with increasing rotation rate during FSW, which will cause coarsening grains in the NZ after FSW. Chowdhury et al. [5] have reported that average grain size of the NZ in the friction stir-welded AZ31 magnesium alloy increased with increasing rotation rate from 1000 to 2000 rpm at a constant welding speed of 20 mm/s. When the rotation rate increased from 500 to 1250 rpm at a constant welding speed of 200 mm/min, the grain size in the NZ could increase gradually for noncombustive Mg-9Al-Zn-Ca magnesium alloy after FSW, as observed by Zhou et al. [21]. No obvious variation is observed for Mg_2Sn phases with increasing rotation rate from 800 to 1100 rpm at a constant welding speed (Fig. 9b–d), which is because the intermetallic phases can be wholly broken into fine particles with tool rotation and friction heat when the rotation rate is between 800 and 1100 rpm.

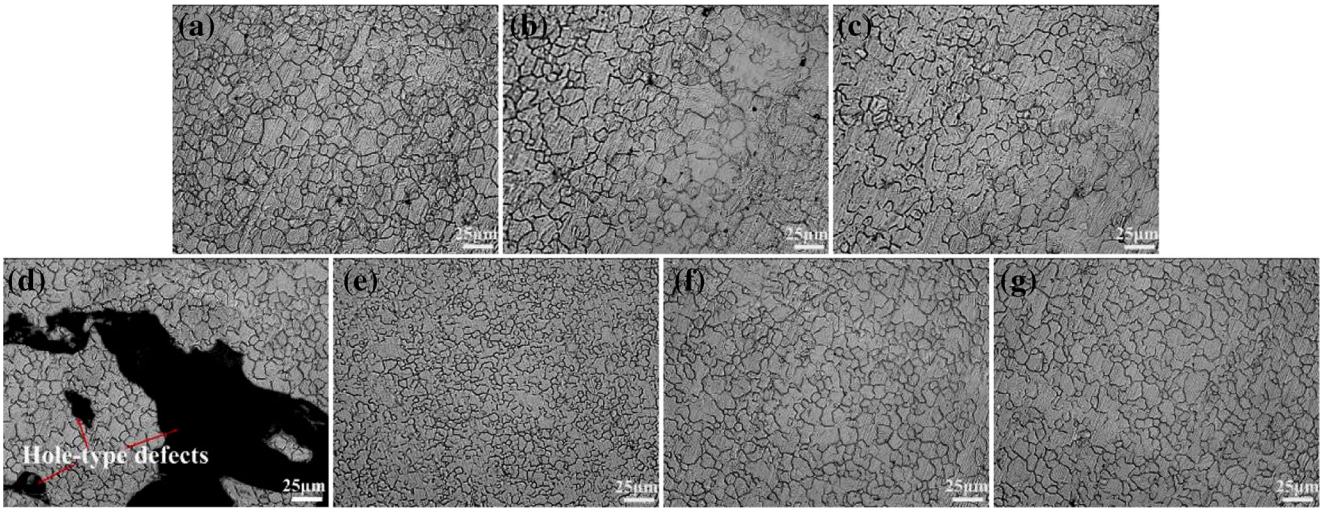

Fig. 8 Optical microscopy images of **a** BM, **b** HAZ at 1000 rpm, **c** TMAZ at 1000 rpm, **d** NZ at 600 rpm, **e** NZ at 800 rpm, **f** NZ at 1000 rpm, and **g** NZ at 1100 rpm

3.2 Hardness distribution

The hardness value of the BM (Fig. 7) fluctuates between 68 and 73 Hv because of the inhomogeneous microstructure of as-extruded plates. After FSW, it is seen that the hardness value in the NZ is slightly higher than that of the BM. That is largely because of the uniform recrystallization refinement of α-Mg matrix and dispersed distribution of Mg_2Sn phase after FSW, although the dissolution of $Mg_{17}Al_{12}$ phase into α-Mg matrix will lower hardness in weld joints. The hardness is greatly influenced by the average grain size according to the Hall-Petch relation [31]. Average grain size of the NZ in friction stir welds decreases compared with the BM, so the hardness value in the NZ is higher than that of the BM.

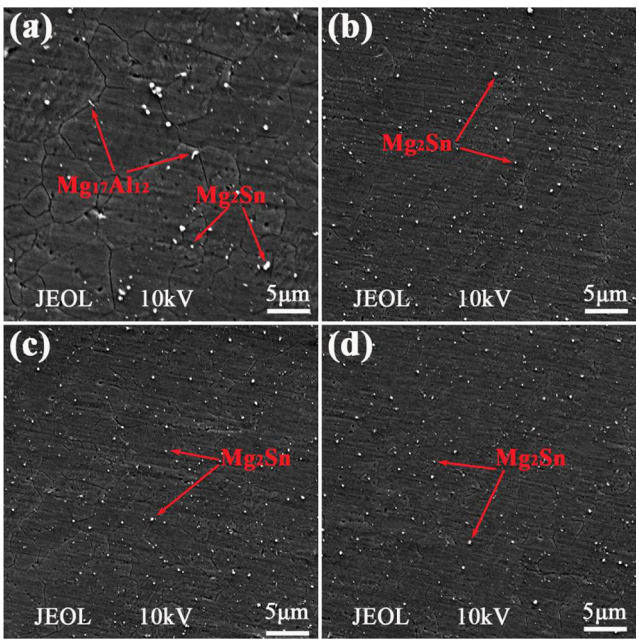

Fig. 9 SEM micrographs of **a** BM, **b** NZ at 800 rpm, **c** NZ at 1000 rpm, and **d** NZ at 1100 rpm

It is also observed that the lowest hardness locates in the region between NZ and TMAZ at the AS but not at RS, without regard to rotation rate. The softness may result from the elongated and deformed grains. As known to all, there is an unsteady material flow around the pin during FSW. At the AS, the temperature is higher than that at RS and the transmutation grains have a greater strain [10]. Dong et al. [32] have reported that the temperature is different at the AS and RS during FSW, and there was lower hardness in the TMAZ at AS.

When the rotation rate increased from 600 to 1100 rpm at a constant welding speed of 150 mm min^{-1}, the hardness profiles have remained more or less unchanged. Perhaps that is because the hardness is relative insensitivity to the change of grain size in certain range. Yang et al. [33] have confirmed that the hardness profiles had little change for the AZ31 magnesium alloy after FSW when the rotation rate increased from 800 to 3500 rpm.

3.3 Tensile properties

All the weld joints after FSW fail with basically 45° shear fracture (Fig. 5), which can be due to the formation of texture by the shear deformation resulting from the rotation of the pin and tool shoulder in that region [34]. It is also seen that the weld joints fail at the boundary between the NZ and TMAZ at AS (Fig. 5). There are three possible reasons for the fracture at the location. The first would be that the texture forms in that location due to strong shear deformation when the pin and tool shoulder rotate during the FSW [34]. Another reason may be that there is the maximum accumulation of basal slip plane (0001) in that region, which can be lead to the minimum Schmid's factor [35]. Thirdly, the fracture location is at the boundary between the NZ and TMAZ at the AS because of the minimum hardness in the region. All the friction stir welds have an uneven distribution of hardness, and the fracture

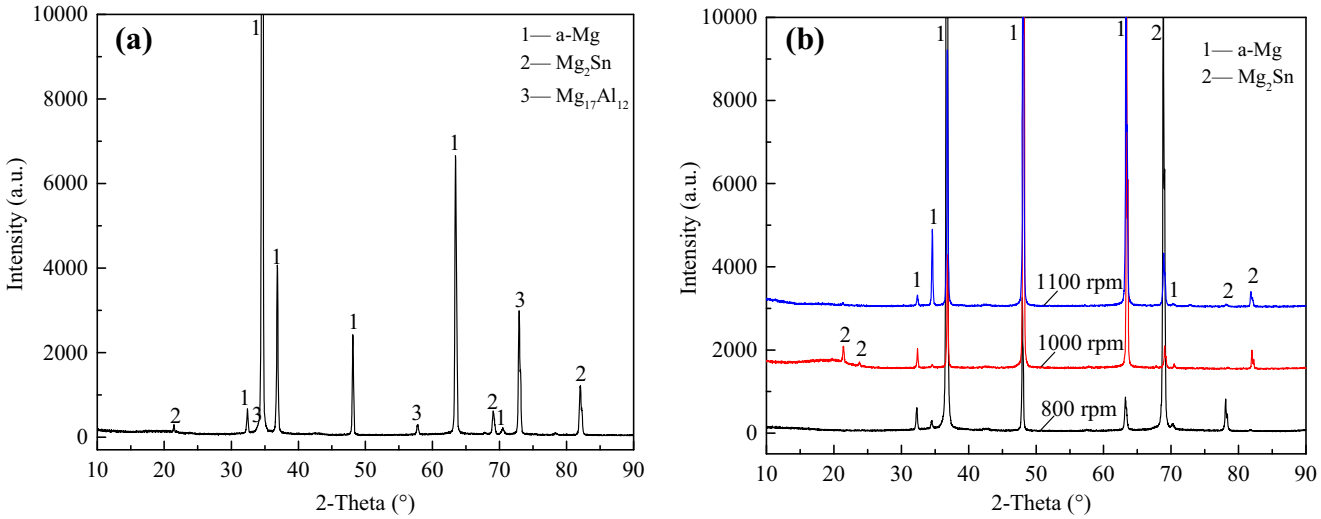

Fig. 10 XRD analysis of **a** the BM and **b** the NZ of weld joints at various rotation rate

location is in the minimum hardness region, which has been confirmed by Ren et al. [36] and Liu et al. [37].

Both the strength and elongation of weld joints decrease compared with the BM (Fig. 4), in which most main reason has four aspects. Firstly, as stated earlier, the alloys with larger grain size have lower hardness on the basis of the Hall-Petch relationship. There is a softened region between NZ and TMAZ of weld joints. The strength is generally proportional to the hardness for magnesium alloy [18], and therefore, the strength of weld joints is lower than that of the BM. Secondly, the lose strength of weld joints may be caused by the dissolution of $Mg_{17}Al_{12}$ intermetallic phases. Moshwan et al. [38] have reported that the dissolution of Mg_2Al_3 intermetallic phases could exhibit significant influence on the decrease of strength for friction stir-welded AA 5052-O aluminum alloy. And, the dissolution of $Mg_{17}Al_{12}$ intermetallic phases had an effect on the strength decrease after FSW for magnesium alloy Mg-5Al-3Sn, as reported by Pan et al. [16]. Thirdly, the residual stress and dislocation density in the TMAZ may influence on the tensile properties of weld joints after FSW, as established by Commin et al. [39, 40]. Fourthly, after FSW, the basal plane could dramatically change, which has a noticeable effect on the tensile properties of weld joints. New crystallographic texture in friction stir-welded magnesium alloys due to the hexagonal close-packed crystal structure can result in the decrease of the strength and elongation of weld joints after FSW, as reported by Park et al. [41]. Pan et al. [16] have reported that the textural variation could lead to a precipitous decline of elongation for friction stir-welded magnesium alloy. Therefore, how to improve the tensile properties of welded joints for Mg-5Al-1Sn alloy after FSW, especially the elongation, will become a study emphasis in further research.

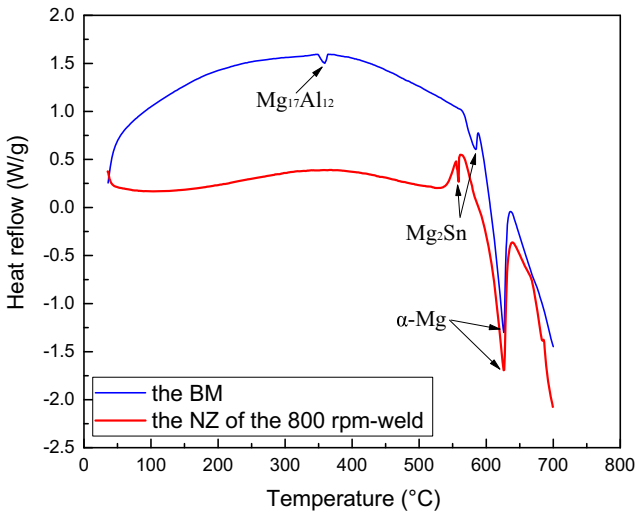

Fig. 11 DSC heating temperature curves of the BM and the NZ in the 800-rpm weld

After FSW, the UTS of weld joints first increases and then decreases when the rotation rate increases from 600 to 1100 rpm at a constant welding speed of 150 mm min^{-1} (Fig. 4). As previously mentioned, at the lower rotation rate of 600 rpm, some hole-type defects are observed in the weld joints induced by insufficient heat and inadequate metal transportation. It is generally known that the tensile strength of weld joints will obviously decrease due to the welding defects. So, the UTS of weld joints at rotation rate of 600 rpm is just 78% of the BM strength, while the UTS of weld joints without obvious defects can reach 87~91% of the BM strength when the rotation rate is between 800 and 1100 rpm.

With increasing rotation rate from 800 to 1100 rpm at a constant welding speed of 150 mm min^{-1}, the UTS of weld joints without welding defects decreases gradually (Fig. 4). This is attributed to different heat generated during FSW. Emam and Domiaty [42] have reported that the total energy per unit length of weld joints varies directly as the rotation rate under a constant of other process parameters. The total energy

per unit length increases with increasing rotation rate, which causes bigger grain size of weld joints. The metal with larger grain size has fewer grain boundaries. Grain boundaries are the major obstacle to dislocation movement. Therefore, there are fewer obstacles to dislocation slip and lower resistance to localized plastic deformation at higher rotation rate during FSW, which will lead to lower tensile strength. Under the common action of multifactors such as crystallographic texture and residual stress, the elongation of weld joints is likely to remain unchanged with increasing rotation rate at a constant welding speed.

4 Conclusions

In the present work, the effects of rotation rate on microstructure and mechanical properties of friction stir-welded Mg-5Al-1Sn magnesium alloy were investigated. The main conclusions are as follows:

(1) At a constant welding speed of 150 mm min^{-1}, Mg-5Al-1Sn magnesium alloy was jointed without defects at rotation rate from 800 to 1100 rpm, while there are hole-type defects at 600 rpm. The weld joint at 800 rpm gave a maximum UTS of 258 MPa, which was 91% of the BM.

(2) After FSW, for Mg-5Al-1Sn magnesium alloy, $Mg_{17}Al_{12}$ phases were with poor thermal stability dissolved into the α-Mg matrix, while Mg_2Sn phases remained in the NZ because of high-dissolution point and good thermal stability.

(3) After FSW, both UTS and elongation of weld joints decreased compared with the BM, which may be caused by the softened region between NZ and TMAZ due to grain growth, the dissolution of $Mg_{17}Al_{12}$ phases, the residual stress and dislocation content in the TMAZ, and the textural variation.

(4) With increasing rotation rate from 600 to 1100 rpm at a constant welding speed of 150 mm min^{-1}, the elongation of weld joints is likely to remain unchanged due to the common action of multifactors, while the UTS first increased and then decreased. Hole-type defects resulted in lower UTS of weld joint at 600 rpm. The UTS of weld joints improved obviously without defects at 800~1100 rpm. When the rotation rate increased from 800 to 1100 rpm, the UTS of weld joints decreased gradually, induced by higher heat generated.

Acknowledgments The present work was supported by the National Natural Science Foundation of China (Project 51531002, 51474043), the Ministry of Education of the People's Republic of China (SRFDR 20130191110018), the International Science and Technology Cooperation Program of China (2010DFR50010-05), Chongqing Municipal Government (CSTC2013JCYJC60001; CEC project, Two River Scholar Project and the Chief Scientist Studio Project), and Chongqing Science and Technology Commission (CSTC2011GJHZ50001, CSTC2013yykfC70003, CSTC2013jjB50006). The authors would like to thank Mr. Peng Peng for providing the experimental materials. Thanks are also due to Mr. Kai Song and Jia She for their assistances during the study.

References

1. Liu LM, Dong CF (2006) Gas tungsten-arc filler welding of AZ31 magnesium alloy. Mater Lett 60:2194–2197. doi:10.1016/j.matlet.2005.12.120
2. Mohammadzadeh Jamalian M, Farahani M, Besharati Givil MK, Aghaei Vafaei M (2016) Study on the effects of friction stir welding process parameters on the microstructure and mechanical properties of 5086-H34 aluminum welded joints. Int J Adv Manuf Technol 83:611–621. doi:10.1007/s00170-015-7581-5
3. He J, Ling ZM, Li HM (2016) Effect of tool rotational speed on residual stress, microstructure, and tensile properties of friction stir welded 6061-T6 aluminum alloy thick plate. Int J Adv Manuf Technol 84:1953–1961. doi:10.1007/s00170-015-7859-7
4. Asadi P, Givi MKB, Akbari M (2016) Simulation of dynamic recrystallization process during friction stir welding of AZ91 magnesium alloy. Int J Adv Manuf Technol 83:301–311. doi:10.1007/s00170-015-7595-z
5. Chowdhury SH, Chen DL, Bhole SD, Cao X, Wanjara P (2013) Friction stir welded AZ31 magnesium alloy: microstructure, texture, and tensile properties. Metall Mater Trans A 44A:323–336. doi:10.1007/s11661-012-1382-3
6. Sahu PK, Pal S (2015) Multi-response optimization of process parameters in friction stir welded AM20 magnesium alloy by Taguchi grey relational analysis. J Magnes Alloy 3:36–46. doi:10.1016/j.jma.2014.12.002
7. Ni DR, Chen DL, Wang D, Xiao BL, Ma ZY (2014) Tensile properties and strain-hardening behaviour of friction stir welded SiCp/AA2009 composite joints. Mater Sci Eng A 608:1–10. doi:10.1016/j.msea.2014.04.060
8. Wang WD, Deng DA, Mao ZT, Tong YG, Ran Y (2016) Influence of tool rotation rates on temperature profiles and mechanical properties of friction stir welded AZ31 magnesium alloy. Int J Adv Manuf Technol online. doi:10.1007/s00170-016-8918-4
9. Commin L, Dumont M, Masse JE, Barrallier L (2009) Friction stir welding of AZ31 magnesium alloy rolled sheets: influence of processing parameters. Acta Mater 57:326–334. doi:10.1016/j.actamat.2008.09.011
10. Cao X, Jahazi M (2009) Effect of welding speed on the quality of friction stir welded butt joints of a magnesium alloy. Mater Des 30:2033–2042. doi:10.1016/j.matdes.2008.08.040
11. Cao X, Jahazi M (2011) Effect of tool rotational speed and probe length on lap joint quality of a friction stir welded magnesium alloy. Mater Design 32:1–11. doi:10.1016/j.matdes.2010.06.048
12. Dobriyal RP, Dhindawa BK, Muthukumaranb S, Mukherjeeb SK (2008) Microstructure and properties of friction stir butt-welded AE42 magnesium alloy. Mater Sci Eng A 477:243–249. doi:10.1016/j.msea.2007.06.028
13. Rao HM, Rodriguez RI, Jordon JB, Barkey ME, Guo YB, Badarinarayan H, Yuan W (2014) Friction stir spot welding of rare-earth containing ZEK100 magnesium alloy sheets. Mater Design 56:750–754. doi:10.1016/j.matdes.2013.12.034
14. Carlone P, Palazzo GS (2015) Characterization of TIG and FSW weldings in cast ZE41A magnesium alloy. J Mater Process Tech 215:87–94. doi:10.1016/j.jmatprotec.2014.07.026
15. Hono K, Mendis CL, Sasaki TT, Oh-ishi K (2010) Towards the development of heat-treatable high-strength wrought Mg alloys. Scripta Mater 63:710–715. doi:10.1016/j.scriptamat.2010.01.038
16. Pan FS, Xu AL, Deng DA, Ye JH, Jiang XQ, Tang AT, Yang R (2016) Effects of friction stir welding on microstructure and

mechanical properties of magnesium alloy Mg-5Al-3Sn. Mater Des 110:266–274. doi:10.1016/j.matdes.2016.07.146
17. Luo AA, Fu PH, Peng LM, Kang XY, Li ZZ, Zhu TY (2012) Solidification microstructure and mechanical properties of cast magnesium-aluminum-tin alloys. Metall Mater Trans A 43:360–368. doi:10.1007/s11661-011-0820-y
18. Elsayed FR, Sasaki TT, Mendis CL, Ohkubo T, Hono K (2013) Compositional optimization of Mg-Sn-Al alloys for higher age hardening response. Mater Sci Eng A 566:22–29. doi:10.1016/j.msea.2012.12.041
19. Kabir ASH, Sanjari M, Su J, Jung I, Yue S (2014) Effect of strain-induced precipitation on dynamic recrystallization in Mg-Al-Sn alloys. Mater Sci Eng A 616:252–259. doi:10.1016/j.msea.2014.08.032
20. Xu AL, Pan FS, Jiang XQ, Li C, Ran Y (2015) Microstructure and properties of friction stir welded Mg-1Al-xSn-0.3Mn magnesium alloys. Mater Sci Forum 816:349–355. doi:10.4028/www.scientific.net/MSF.816.349
21. Zhou L, Nakata K, Liao J, Tsumura T (2012) Microstructural characteristics and mechanical properties of non-combustive Mg-9Al-Zn-Ca magnesium alloy friction stir welded joints. Mater Design 42:505–512. doi:10.1016/j.matdes.2012.06.005
22. Lohwasser D, Chen Z (2010) Friction stir welding from basics to applications. Woodhead Publishing Limited and CRC Press LLC, Boca Raton, pp. 15–17
23. Park SHC, Sato YS, Kokawa H (2003) Effect of micro-texture on fracture location in friction stir weld of Mg alloy AZ61 during tensile test. Scripta Mater 49:161–166. doi:10.1016/s1359-6462(03)00210-0
24. Afrin N, Chen DL, Cao X, Jahazi M (2008) Microstructure and tensile properties of friction stir welded AZ31B magnesium alloy. Mater Sci Eng A 472:179–186. doi:10.1016/j.msea.2007.03.018
25. Yang J, Xiao BL, Wang D, Ma ZY (2010) Effects of heat input on tensile properties and fracture behavior of friction stir welded Mg–3Al–1Zn alloy. Mater Sci Eng A 527:708–714. doi:10.1016/j.msea.2009.09.044
26. Albakri AN, Mansoor B, Nassar H, Khraisheh MK (2013) Thermo-mechanical and metallurgical aspects in friction stir processing of AZ31 Mg alloy—a numerical and experimental investigation. J Mater Process Tech 213:279–290. doi:10.1016/j.jmatprotec.2012.09.015
27. Darras BM, Khraisheh MK, Abu-Farha FK, Omar MA (2007) Friction stir processing of commercial AZ31 magnesium alloy. J Mater Process Tech 191:77–81. doi:10.1016/j.jmatprotec.2007.03.045
28. Mironov S, Onuma T, Sato YS, Kokawa H (2015) Microstructure evolution during friction-stir welding of AZ31 magnesium alloy. Acta Mater 100:301–312. doi:10.1016/j.actamat.2015.08.066
29. Ji SD, Shi QY, Zhang LG, Zou AL, Gao SS, Zan LV (2012) Numerical simulation of material flow behavior of friction stir welding influenced by rotational tool geometry. Comput Mater Sci 63:218–226. doi:10.1016/j.commatsci.2012.06.001
30. Chai F, Zhang DT, Li YY, Zhang W (2015) Microstructure evolution and mechanical properties of a submerged friction-stir-processed AZ91 magnesium alloy. J Mater Sci 50:3212–3225. doi:10.1007/s10853-015-8887-2
31. Motallebnejad P, Saeid T, Heidarzadeh A, Darzi KH, Ashjari M (2014) Effect of tool pin profile on microstructure and mechanical properties of friction stir welded AZ31B magnesium alloy. Mater Des 59:221–226. doi:10.1016/j.matdes.2014.02.068
32. Dong P, Li HM, Sun DQ, Gong WB, Liu J (2013) Effects of welding speed on the microstructure and hardness in friction stir welding joints of 6005A-T6 aluminum alloy. Mater Design 45:524–531. doi:10.1016/j.matdes.2012.09.040
33. Yang J, Wang D, Xiao BL, Ni DR, Ma ZY (2013) Effects of rotation rates on microstructure, mechanical properties, and fracture behavior of (FSW) AZ31 magnesium alloy. Metall Mater Trans A 44A:517–530. doi:10.1007/s11661-012-1373-4
34. Pareek M, Polar A, Rumiche F (2006) Proceedings of the seventh international conference on trends in welding research. ASM International GA, United State, May 16-20:421–426
35. Woo W, Choo H, Brown DW, Liaw PK, Feng Z (2006) Texture variation and its influence on the tensile behavior of a friction-stir processed magnesium alloy. Scripta Mater 54:1859–1864. doi:10.1016/j.scriptamat.2006.02.019
36. Ren SR, Ma ZY, Chen LQ (2007) Effect of welding parameters on tensile properties and fracture behavior of friction stir welded Al–Mg–Si alloy. Scripta Mater 56:69–72. doi:10.1016/j.scriptamat.2006.08.054
37. Liu HJ, Fujii H, Maeda M, Nogi K (2003) Mechanical properties of friction stir welded joints of 1050-H24 aluminium alloy. Sci Technol Weld Join 8:450–454
38. Moshwan R, Yusof F, Hassan MA, Rahmat SM (2015) Effect of tool rotational speed on force generation, microstructure and mechanical properties of friction stir welded Al-Mg-Cr-Mn (AA 5052-O) alloy. Mater Design 66:118–128. doi:10.1016/j.matdes.2014.10.043
39. Commin L, Dumontb M, Rotinata R, Pierrona F, Massec JE, Barrallierc L (2012) Influence of the microstructural changes and induced residual stresses on tensile properties of wrought magnesium alloy friction stir welds. Mater Sci Eng A 551:288–292. doi:10.1016/j.msea.2012.05.021
40. Commin L, Dumont M, Masse JE, Barrallier L (2009) Friction stir welding of AZ31 magnesium alloy rolled sheets: influence of processing parameters. Acta Mater 57:326–334. doi:10.1016/j.actamat.2008.09.011
41. Park SHC, Sato YS, Kokawa H (2003) Basal plane texture and flow pattern in friction stir weld of a magnesium alloy. Metall Mater Trans A 34A:987–994. doi:10.1007/s11661-003-0228-4
42. Emam SA, Domiaty AE (2009) A refined energy-based model for friction-stir welding. Proceedings of world Academy of Science. Eng Technol 53:1016–1022